Atmos. Chem. Phys. Discuss., 3, 3681–3711, 2003
www.atmos-chem-phys.org/acpd/3/3681/

Atmospheric Chemistry and Physics Discussions

Impact of high solar zenith angles on dynamical and chemical processes in a coupled chemistry-climate model

D. Lamago[1,*], M. Dameris[1], C. Schnadt[1], V. Eyring[1], and C. Brühl[2]

[1]Institut für Physik der Atmosphäre, DLR-Oberpfaffenhofen, D-82234 Wessling, Germany
[2]Max-Planck-Institut für Chemie, D-55020 Mainz, Germany
[*]Now at: ZWE FRM-II and Institut für Experimentalphysik E21, TU-München, D-85748 Garching, Germany

Received: 4 June 2003 – Accepted: 11 July 2003 – Published: 22 July 2003

Correspondence to: M. Dameris (Martin.Dameris@dlr.de)

Abstract

Actinic fluxes at high solar zenith angles (SZAs) are important for atmospheric chemistry, especially under twilight conditions in polar winter and spring. The results of a sensitivity experiment employing the fully coupled 3D chemistry-climate model ECHAM4.L39(DLR)/CHEM have been analysed to quantify the impact of SZAs greater than 87.5° on dynamical and chemical processes in the lower stratosphere, in particular their influence on the ozone layer.

Although the actinic fluxes at SZAs larger than 87.5° are small, ozone concentrations are significantly affected because daytime photolytic ozone destruction is switched on earlier, especially the conversion of Cl_2 and Cl_2O_2 into ClO at the end of polar night in the lower stratosphere. Comparing climatological mean ozone column values of a simulation considering SZAs up to 93° with those of the sensitivity run with SZAs confined to 87.5° total ozone is reduced by about 20% in the polar Southern Hemisphere, i.e., the ozone hole is "deeper" if twilight conditions are considered in the model because there is 2–3 weeks more time for ozone destruction. This causes an additional cooling of the polar lower stratosphere (50 hPa) up to −4 K with obvious consequences for chemical processes. In the Northern Hemisphere the impact of high SZAs cannot be determined on the basis of climatological mean values due to the pronounced dynamic variability of the stratosphere in winter and spring.

1. Introduction

Chemistry-climate links have received increased attention in recent years (IPCC, 2001; EC, 2003; WMO, 2003). The investigation of mutual effects of dynamical, chemical, and radiative coupling in the Earth's atmosphere is currently an outstanding scientific issue. Improved knowledge is necessary to better understand the relations between changes in atmospheric composition and climate. One key question, for example, is to which extent the recent destruction of the ozone layer has been affected by radiative

ACPD

3, 3681–3711, 2003

cooling of the stratosphere due to increased greenhouse gas concentrations and how this will influence future ozone recovery.

Fully coupled three-dimensional (3D) chemistry-climate models (CCMs) are suitable tools to investigate the importance of these mutual effects. CCMs have been used to simulate the recent and future development of the chemical composition and the dynamics of the atmosphere (e.g. Rozanov et al., 2001; Austin, 2002; Schnadt et al., 2002; Nagashima et al., 2002; Pitari et al., 2002; Steil et al., 2003). The uncertainties and assessments of the currently available CCMs have been recently summarised by Austin et al. (2003).

In this study the CCM ECHAM4.L39(DLR)/CHEM (hereafter E39/C) is employed to assess the impact of solar zenith angles (SZAs) greater than 87.5° for the chemistry and dynamics of the lower stratosphere, in particular at polar latitudes during winter and spring. It is well-known that the impact of photolysis on mixing ratios of chemical species depends on the maximum SZA allowed in model calculations. For example, an estimate by the 2D chemistry model MPIC for a specific case study at the 475 K isentropic level showed that the total percentage ozone loss increased from 25% to 31% when the maximum SZA was raised from 90° to 92° (Krämer et al., 2003). Moldanova et al. (2002) showed that for some halogenated species and NO_3, the photolysis beyond 90° SZA may be of importance. Nevertheless, some CCMs neglect the impact of twilight for simplicity reasons, which certainly has an impact on chemical processes, especially during winter and spring near the edge of the polar night.

This paper aims to quantify the effect of photolysis beyond 87.5° SZA in a fully coupled 3D CCM. In the next section the employed model system E39/C is briefly described, with special focus on the parameterisation for the photolysis to 93° SZA used here. The numerical simulations forming the basis for this investigation are briefly introduced. In Sect. 3 the model results are discussed, i.e., changes of photolysis frequencies, of ozone mixing ratios, and of related dynamical and chemical effects. Our conclusions are presented in the last section.

ACPD
3, 3681–3711, 2003

2. Model description and design of experiments

2.1. Brief description of E39/C

In this study the interactively coupled chemistry-climate model E39/C is employed. More detailed descriptions of the model are given in Hein et al. (2001) and Schnadt et al. (2002). The model horizontal resolution is T30. In the vertical, E39/C has 39 layers from the surface to the top layer centred at 10 hPa (Land et al., 2002). The chemistry modul CHEM (Steil et al., 1998) is based on the family concept. It describes relevant stratospheric and tropospheric O_3 related homogeneous chemical reactions and heterogeneous chemistry on polar stratospheric clouds (PSCs) and sulphate aerosols, it does not consider bromine chemistry. E39/C includes an online feedback of chemistry, dynamics, and radiative processes. Chemical tracers are advected by the simulated winds. The net heating rates, in turn, are calculated using the actual 3D distributions of the radiatively active gases O_3, CH_4, N_2O, H_2O, and CFCs. Climatological means of dynamical and chemical fields have been intensively validated with regards to other model results and to observations (e.g., Austin et al., 2003; Land et al., 2002; Hein et al., 2001).

2.2. Parameterisation of photolysis frequencies at high SZAs

The photolysis frequencies for SZAs less equal 87.5° are calculated using the efficient method of Landgraf and Crutzen (1998) (see also Landgraf, 1998). The spectral range (178.6 nm $\leq \lambda \leq$ 752.5 nm) relevant for the photo-chemistry of the troposphere and the middle atmosphere is divided into 8 wavelength intervals $I_i (i = 1, \ldots, 8)$. For each interval, the photolysis frequency $J_{i,x}$ of a gas x is calculated according to the equation:

$$J_{i,x} = \int_{I_i} \sigma_x(\lambda)\Phi_x(\lambda)F(\lambda)d\lambda, \quad (1)$$

ACPD
3, 3681–3711, 2003

where $\sigma_x(\lambda)$ is the absorption cross section, $\Phi_x(\lambda)$ the quantum yield, and $F(\lambda)$ the actinic flux in the interval I_i. In the spectral range of 202.0 nm $\leq \lambda \leq$ 752.5 nm, scattering at air molecules, aerosols, and clouds is not negligible. To include this efficiently, $J_{i,x}$ is calculated from precalculated photolysis frequencies for a purely absorbing atmosphere using Eq. (1) with high spectral resolution and a correction factor for the scattering effects:

$$J_{i,x} = J^a_{i,x}\delta_i \tag{2}$$

with

$$\delta_i = \frac{F(\lambda_i)}{F^a(\lambda_i)}. \tag{3}$$

$F^a(\lambda_i)$ and $F^a(\lambda)$ (see Eq. 4) are the actinic fluxes for a purely absorbing atmosphere for the wavelength λ_i and λ in the interval I_i. They are calculated using the Lambert-Beer absorption law:

$$F^a(\lambda) = F_0(\lambda) exp\{-\sum_k V_k \sigma_k(\lambda)\}, \tag{4}$$

where $F_0(\lambda)$ is the spectral solar irradiance at the model top, V_k is the slant column, and σ_k is the absorbtion cross section of the kth absorber (O_2 and O_3). The correction factor δ_i is calculated online with a radiative transfer code (Zdundowski et al., 1980) at λ_i of Landgraf and Crutzen (1998). It takes into account scattering as well as absorption due to air molecules, aerosols, clouds, and the Earth's surface. The photolysis frequency is determined by the following equation:

$$J_x \approx J^a_{1,x} + \sum_{i=2}^{8} J^a_{i,x}\delta_i. \tag{5}$$

Here, $J^a_{1,x}$ is the photolysis frequency in the spectral range of the Schumann-Runge band (178.6 nm$\leq \lambda \leq$ 202.0 nm), where O_2 is a strong absorber and scattering can

be neglected. So far, $J^a_{i,x}$ is calculated for an isothermal atmosphere. To account for the temperature dependence of σ and Φ, a correction function is applied. For further details of the parametrisation of $J^a_{i,x}$ and the temperature dependence see Landgraf (1998). Equations (1) to (5) are valid for SZAs to 87.5°. For greater SZAs, the parameterisation of photolysis frequencies is done according to the laws of spherical geometry, where the actinic flux for a given wavelength depends on the SZA θ (Levy II, 1974). Röth (1992, 2002) introduced the following empirical formula for photolysis frequencies which includes very large zenith angles:

$$J = J_0 \cdot exp[b(1 - sec(c\theta))], \tag{6}$$

with J_0 photolysis frequency for overhead sun and standard atmosphere at a certain altitude and empirical coefficients b and c which are tabulated for all species of interest. In E39/C we modify and split this fit to account for the interactively calculated atmospheric quantities like ozone columns and reflection from clouds by adopting the J-value at SZA 87.5° obtained in Landgraf and Crutzen (1998) multiplied with a correction function:

$$J_{>87.5} = J_{87.5} \cdot F_{corr} \tag{7}$$

with

$$F_{corr} = exp[19.09 b_i (1 - \frac{\theta}{87.5})]. \tag{8}$$

The empirical coefficients b_i are species dependent and listed in Table 1. For SZAs between about 70° and 90° for the airmass factor d(θ) used in photolysis calculation an empirical correction for the curvature of the atmosphere based on the Chapman-function is applied (e.g. Lacis and Hansen, 1974):

$$d(\theta) = \frac{35}{\sqrt{1224 \cos^2 \theta + 1}}. \tag{9}$$

ACPD
3, 3681–3711, 2003

For smaller SZAs this formula converges to $1/\cos\theta$.

This technique allows to calculate the photolysis rates online in a realistic atmospheric state, in which the SZA is time dependent.

2.3. Model experiments

Two timeslices representing atmospheric conditions for the early 1990s have been used, namely, a control scenario including SZAs up to 93° (SZA93) and a sensitivity simulation which does not consider SZAs greater than 87.5° (SZA87.5) (see Sect. 2.2). Each timeslice has been integrated over 24 years under steady state conditions with the first four years taken as spin-up. For both model simulations, climatological mean sea surface temperatures (SST) are prescribed from observations for the years 1979 to 1994 (Gates, 1992). In addition, natural and anthropogenic NO_x emissions are fixed at the surface. At the model top, mixing ratios of NO_y and ClX (=ClO_x + $ClONO_2$ + HCl) are prescribed to account for higher altitude chemistry above the upper boundary. Moreover, mixing ratios for the most relevant greenhouse gases CO_2, CH_4, and N_2O are fixed for each scenario. They are specified according to observations for the year 1990. The specific boundary conditions are summarised in Table 2.

3. Discussion of results

3.1. Changes of photolysis frequencies

Neglecting high SZAs is associated with less photons at the day-night transition and in particular with a delay of daytime chemistry at the end of the polar night with significant effects for the destruction of ozone in the polar lower stratosphere. The photolysis of heterogeneously formed Cl_2 at large SZAs after polar night initiates the catalytic ozone destruction by chlorine. Ozone depletion rates are highly related to the photolyis rates of Cl_2O_2 ($\rightarrow O_2 + 2Cl$).

Figure 1 shows the absolute values of the photolysis frequencies of Cl_2O_2 for a single model year at 50 hPa of the simulation SZA93. The structure of this field obviously reflects the importance of ozone as the dominant absorber: the photolysis frequencies are enhanced southward of 60°S between October and November (more than $1.2{\cdot}10^{-3}$ s^{-1}), when ozone column values are still small and actinic fluxes differ significantly from zero. Including SZAs higher than 87.5° leads to changes in the photolysis frequencies of Cl_2O_2 as is displayed in Fig. 2 for the 50 hPa level. As expected, the most obvious changes are detected at the edge of the polar night (up to $0.6{\cdot}10^{-4}$ s^{-1}) in both hemispheres (approx. 10%). Absolute differences of the same order of magnitude are found in the Southern Hemisphere in the polar region at the end of November, which is about 5%. This indicates enhanced actinic fluxes at that time due to reduced ozone (see Sect. 3.2).

3.2. Change of ozone

3.2.1. Ozone columns

In order to evaluate the impact of twilight on upper tropospheric and lower stratospheric chemistry, we first compare the results of the climatological mean total ozone averaged over 20 simulated years including solar zenith angles up to 93° (SZA93) (Fig. 3) to the values of a simuation that only considered SZAs up to 87.5° (SZA87.5) (Fig. 4). Figure 5 shows the differences between the modelled climatological mean total ozone fields (SZA93-SZA87.5). In the southern mid- and high latitudes between 40°S and 90°S the largest ozone difference values are simulated. These differences are statistically significant due to the relative low inter-annual variability (Fig. 6). The ozone reduction is strongest between September and November due to the photon surplus in SZA93. The maximum differences are found in the core region of the polar vortex. At the end of September approximately 30 Dobson Units (DU) less ozone are found in the SZA93 case. This corresponds to a maximum reduction of the ozone column over the south polar region of about 20% in the SZA93 run in comparison to the SZA87.5

ACPD
3, 3681–3711, 2003

simulation. Additionally, a closer inspection of Figs. 3 and 4 shows that in the SZA93 case a faster ozone depletion is detected in August and September. The ozone hole (i.e., first detection of total ozone values less than 220 DU) appears approximately 2 weeks earlier than in the SZA87.5 run. The lifetime of the ozone hole is about one week longer in the SZA93 run.

In the Northern Hemisphere total ozone is moderately increased by about 2% to 4% between February and the middle of March. Due to the high inter-annual dynamic variability of the Northern Hemisphere polar stratosphere (Fig. 6), however, the changes are not statistically significant in this region. Hence the Arctic climatological mean ozone column is only slightly affected by high SZAs. This does not principally exclude that individual cold Northern Hemisphere model winters experience similar high SZA effects as is generally found in the Southern Hemisphere, i.e., enhanced ozone depletion caused by an earlier sunrise (consideration of twilight photochemistry). Rex et al. (2003) showed, that photochemical box model calculations cannot fit observed ozone loss rates during cold Arctic Januaries. There are hints that the missing ozone loss mechanism is most important at high SZAs and low temperatures.

In tropical regions, as well as in midlatitudes only small changes occur due to higher SZAs. The differences in these regions are about 1% (approximately 3 DU) of the total ozone column, they are statistically not significant. This can be explained considering the mean ozone value of about 275 DU per year in the tropics and the very low inter-annual dynamic variability in these regions (Fig. 6).

3.2.2. Zonal mean ozone difference

To investigate the modelled ozone changes due to high SZAs in more detail, differences of zonal mean ozone mixing ratios are presented in Fig. 7 showing changes for January, April, July, and October. Nearly no changes of ozone mixing ratios are calculated below 150 hPa, most of the differences occur in the stratosphere. Ozone mixing ratios significantly decrease during southern spring at levels between 100 hPa and the model top. In SZA93, additional ozone decreases are mainly detected inside the polar vortex

ACPD
3, 3681–3711, 2003

(south of ∼65° S). At the centre of the polar vortex, between 70 hPa and 10 hPa an ozone reduction of more than −500 ppbv is found in October. As already noted, sun rays enter the model atmosphere region between 65°S and the South pole earlier in spring in SZA93 than in SZA87.5. The photon surplus at the edge of the polar night is responsible for the increased ozone destruction (see Sect. 3.1).

At midlatitudes and in the tropical regions, ozone decreases are larger at the upper model levels than at lower levels. Ozone differences up to −50 ppbv are simulated in January between 60° S and 10° S and between 30 hPa and 10 hPa. Because of the ozone reduction at the upper model levels, more sunlight penetrates down to lower atmospheric layers which has an impact on dynamics (temperature) and chemistry. Ozone differences are small in the equatorial regions. In April and July, ozone concentrations are larger in SZA93 by about 20 ppbv in comparison to SZA87.5. This is probably due to a slightly distinct circulation pattern producing small differences in the climatological mean ozone distributions in both model experiments (Sect. 3.3).

The Arctic stratosphere shows some modifications in ozone mixing ratios, however, these changes are mostly not statistically significant due to the high dynamic interannual variability of the Northern Hemisphere (Fig. 6). The described ozone changes caused by considering high SZAs are due to dynamical and chemical effects. In the next two sections we will quantify some of these effects in the applied CCM.

3.3. Change of dynamics

Statistically significant temperature differences between the SZA93 and the SZA87.5 simulations are mainly found in the extra-tropical Southern Hemisphere lower stratosphere (between 10 and 100 hPa). Figure 8 shows the differences for the 50 hPa pressure level. The largest values occur during polar spring (up to −4 K) indicating that the SZA93 simulation produces colder conditions there. Near the edge of the Southern Hemisphere polar vortex the SZA93 run shows a cooling between −0.5 K and −1 K. These temperature differences can be easily related to the detected changes of the ozone column between the two model runs discussed in the last two sections (Fig. 5).

In SZA93, the stratosphere is colder in regions with reduced ozone columns with regards to the SZA87.5 run. In the Northern Hemisphere, higher temperatures are found in the SZA93 case in later winter and early spring in the polar region due to the increase of total ozone. As mentioned before, these differences are statistically not significant due to the high dynamic inter-annual variability in this time of the year and region. Therefore, these temperature differences are fortuitous and cannot be interpreted. The increase of the ozone column in the tropics in the SZA93 run (i.e., about 2 DU in May and June, cf. Fig. 6) produces a warming of approximately 0.7 K. Although these differences are small they are statistically significant because the inter-annual variability in the equatorial region is very small (see also Fig. 6).

The differences in the temperature fields result in corresponding differences in the mean zonal wind fields (not shown). However, these are statistically not significant, neither in the Southern nor in the Northern Hemisphere. For example, the Southern Hemisphere polar night jet is stronger in the SZA93 simulation by about 2 m/s. In the Northern Hemisphere, the wintertime stratospheric polar vortex is weaker (about −2 m/s) in SZA93. These results are consistent with the formerly discussed ozone and temperature differences.

Altogether it can be summarised that the mean climatological temperature conditions are clearly different in the polar Southern Hemisphere. This has a strong impact on the temperature-dependent chemistry, in particular on the formation of polar stratospheric clouds (PSCs) and thus the ozone destroying heterogeneous chemical processes (see Sect. 3.4).

3.4. Change of chemistry

To estimate the importance of considering SZAs greater than 87.5° on stratospheric chemistry in a fully coupled 3D CCM, some chemical species have been analysed which are especially relevant for polar chemistry. In the following, we concentrate on Southern Hemisphere winter and spring conditions where the differences of climatological mean fields between the two model simulations are most obvious. For an

appropriate presentation of the results, the zonal mean values derived from the standard coordinate system are transformed to a description employing equivalent potential vorticity (PV) coordinates (e.g. Butchart and Remsberg, 1986; Manney et al., 1994).

As shown in the previous section, stratospheric temperatures are reduced if SZAs up to 93° are considered. Main temperature differences between the SZA93 run and the SZA87.5 simulation are found in springtime inside the polar vortex. This favours the formation of PSCs in the SZA93 run. In this region the conditions are most favourable for heterogenous chemistry on PSC surfaces during the polar night. Figures 9 and 10 show the differences of PSC I and II mixing ratios between the two simulations at 50 hPa. Obviously, a statistically significant increase of NAT and ice particles can be found in SZA93 reflecting the differences in temperatures. Both figures illustrate that the enhancement is firstly seen at the inner edge of the polar vortex in mid-winter. Maximum differences are shifted towards higher latitudes with time with the size of the polar vortex becoming smaller.

The photon surplus increases the photolysis of chlorine products (Cl_2, HOCl, and $ClONO_2$) in SZA93. ClO and Cl radicals are released and enhance the destruction of ozone through catalytic reactions. Figure 11 shows the differences in ClO_x at the 50 hPa pressure level. An enhanced activation of chlorine is found inside the polar vortex between July and November. Maximum difference values are about 0.5 ppbv, these differences are statistically significant. An exception is found in the core region of the polar vortex in the second half of October where a decrease of ClO_x (up to −0.3 ppbv) is detetected in the SZA93 run. This behaviour can be explained considering the related differences of $ClONO_2$ and HCl which are displayed in Figs. 12 and 13. Reduced $ClONO_2$ mixing ratios are found in the SZA93 run inside the polar vortex between mid October and mid November while HCl is increased there. (The collar of $ClONO_2$ is enhanced in the SZA93 simulation, as expected.) The chemical reaction $Cl + O_3 \rightarrow ClO + O_2$ determines the rate of formation of $ClONO_2$: if only little ozone (0.5 ppbv or less) is available, less chlorine monoxide (ClO) is produced which can be transformed to $ClONO_2$ ($ClO + NO_2 + M \rightarrow ClONO_2 + M$). In this case, an

increased formation of HCl is found ($Cl + CH_4 \rightarrow HCl + CH_3$). Thus, the chlorine atoms formed by the photolysis of Cl_2 and Cl_2O_2 after mid October do not primarily react with ozone, but with methane increasing HCl. This model behaviour is in agreement with box model calculations and HALOE observations (Grooß et al., 1997).

4. Conclusions

The current sensitivity study with a fully coupled CCM has shown that photolysis reactions during twilight have a non-negligible impact on the lower stratosphere, although the actinic fluxes for SZAs greater 87.5° are small. Considering climatological mean values, statistically significant effects on the chemistry and dynamics of the lower stratosphere are mainly found in higher latitude regions of the Southern Hemisphere during winter and spring. Due to the high dynamic variability of the Northern Hemisphere stratosphere, similar effects cannot be detected there. Certainly, in individual cold Northern Hemisphere winter periods with a stable polar vortex analogous results would be obtained. The detected changes of dynamic and chemical values in the tropics and mid-latitude regions can be neglected.

In E39/C, the small surplus of photons for SZAs greater 87.5° produces a different climatological mean ozone distribution. In the SZA93 run, ozone destruction is stronger, particularly at the edge of the polar night. The maximum effect is found near the South Pole in spring. Due to reduced ozone concentrations, less UV radiation is absorbed in SZA93. This cools down the lower stratosphere, causing an increased formation of PSCs. Consequently, heterogeneous chemical reactions on PSC particles, subsequent chlorine activation, and ozone destruction are intensified. In the Southern Hemisphere, this results in a total additional reduction of the climatological mean total ozone column of approximately 20% and an extension of the “ozone hole season” of about three weeks.

This study is the first assessment using a 3D CCM to quantify the effects of high

SZAs on the dynamics and chemistry of the lower stratosphere. It shows that the photolysis for SZAs greater 87.5° is relevant especially in polar regions and cannot be neglected for simplicity reasons as partially done in other CCMs.

Acknowledgements. The authors thank Ernst-Peter Röth for helpful comments. The work was partly supported by the German Government (BMBF) within the scope of the AFO 2000 project KODYACS.

References

Austin, J.: A three-dimensional coupled chemistry-climate model simulation of past stratospheric trends, J. Atmos. Sci., 59, 218–232, 2002. 3683

Austin, J., Shindell, D., Beagley, S. R., Brühl, C., Dameris, M., Manzini, E., Nagashima, T., Newman, P., Pawson, S., Pitari, G., Rozanov, E., Schnadt, C., and Shepherd, T. G.: Uncertainties and assessments of chemistry-climate models of the stratosphere, Atmos. Chem. Phys., 3, 1–27, 2003. 3683, 3684

Butchart, N. and Remsberg, E. E.: The area of the stratospheric polar vortex as a diagnostic for tracer transport on an isentropic surface, J. Atmos. Sci., 43, 1319–1339, 1986. 3692

EC: European report on ozone-climate interactions, in press, 2003. 3682

Gates, W. L.: AMIP: The atmospheric model intercomparison project, Bull. Amer. Meteor. Soc., 73, 1962–1970, 1992. 3687

Grooß, J.-U., Bradley, R. B., Crutzen, P. J., Grose, W. L., and Russell III, J. M.: Re-formation of chlorine reservoirs in southern hemisphere polar spring, J. Geophys. Res., 102, 13 141–13 152, 1997. 3693

Hein, R., Dameris, M., Schnadt, C., Land, C., Grewe, V., Köhler, I., Ponater, M., Sausen, R., Steil, B., Landgraf, J., Brühl, C.: Results of an interactively coupled atmospheric chemistry-general circulation model: Comparison with observations, Ann. Geophysicae, 19, 435–457, 2001. 3684

IPCC (Intergovernmental Panel on Climate Change): Climate change 2001; the scientific basis, contribution of working group I to the Third Assessment Report of IPCC, Houghton, J. T., Ding, Y., Griggs, D. J., Noguer, M., van der Linden, P. J., Dai, X., Maskell, K., and Johnson, C. A. (Eds), Cambridge University Press, 2001. 3682

Krämer, M., Müller, Ri., Bovensmann, H., Burrows, J., Brinkmann, J., Röth, E. P., Grooß, J.-U., Müller, Ro., Woyke, T., Ruhnke, R., Günther,G., Hendricks, J., Lippert, E., Carslaw, K. S., Peter, T., Zieger, A., Brühl, C., Steil, B., Lehmann, R., and McKenna, D. S.: Intercomparison of stratospheric chemistry models under polar vortex conditions, J. Atmos. Chem., in press, 2003. 3683

Lacis, A. A. and Hansen, J. E.: A parameterization for the absorption of solar radiation in the Earth's atmosphere, J. Atmosph. Sci., 31, 118–133, 1974. 3686

Land, C., Feichter, J., and Sausen, R.: Impact of vertical resolution on the transport of passive tracers in the ECHAM4 model, Tellus, 54B, 344–360, 2002. 3684

Landgraf, J.: Modellierung photochemisch relevanter Strahlungsvorgänge in der Atmosphäre unter Berücksichtigung des Einflusses von Wolken, Fachbereich Physik, Universität Mainz, Ph.D. thesis, 1998. 3686

Landgraf, J. and Crutzen, P. J.: An efficient method for online calculations of photolysis and heating rates, J. Atmos. Sci., 55, 863–878, 1998. 3684, 3685, 3686

Levy II, H.: Photochemistry of the troposphere, Adv. Photochem., 9, 369–524, 1974. 3686

Manney, G. L., Zurek, R. W., Gelman, M. E., Miller, A. J., Nagatani, R.: The anomalous Arctic lower stratospheric polar vortex, Geophys. Res. Lett., 21, 2405–2408, 1994. 3692

Moldanova, J., Bergström, R., and Langner, J.: A photolysis scheme for photochemical modelling of the troposphere and lower stratosphere, A contribution to the EUROTRAC-2 subproject GLOREAM, Proceedings from the EUROTRAC-2 Symposium, Garmisch-Partenkirchen, 2002. 3683

Nagashima, T., Takahashi, M., Takigawa, M., and Akiyoshi, H.: Future development of the ozone layer calculated by a general circulation model with fully interactive chemistry, Geophys. Res. Lett., 10.1029/2001GL014026, 2002. 3683

Pitari, G., Manzini, E., Rizi, V., and Shindell, D.: Impact of future climate and emission changes on stratospheric aerosols and ozone, J. Atmos. Sci., 59, 414–440, 2002. 3683

Rex, M., Salawitch, R. J., Santee, M. L., Waters, J. W., Hoppel, K., and Bevilacqua, R.: On the unexplained stratospheric ozone losses during cold Arctic Januaries, Geophys. Res. Lett., 30, 1008, doi 10.1029/2002GL016008, 2003. 3689

Röth, E.-P.: A fast algorithm to calculate the photonflux in optically dense media for use in photochemical models, Ber. Bunsenges. Phys. Chem., 96, 417–420, 1992. 3686

Röth, E.-P.: Description of the Anisotropic Radiation Transfer Model ART to Determine Photodissociation Coefficients, Institut für Stratosphärische Chemie, Forschungszentrum Jülich,

2002. 3686
Rozanov, E. V., Schlesinger, M. E., and Zubov, V. A.: The Universtiy of Illinois at Urbana-Champaign three-dimensional stratosphere-troposphere general circulation model with interactive ozone photochemistry: Fifteen-year control run climatology, J. Geophys. Res., 106, 27 233–27 254, 2001. 3683
Schnadt, C., Dameris, M., Ponater, M., Hein, R., Grewe, V., and Steil, B.: Interaction of atmospheric chemistry and climate and its impact on stratospheric ozone, Clim. Dyn., 18, 501–517, 2002. 3683, 3684
Steil, B., Dameris, M., Brühl, C., Crutzen, P. J., Grewe, V., Ponater, M., and Sausen, R.: Development of a chemistry module for GCMs: first results of a multiannual integration, Ann. Geophysicae, 16, 205–228, 1998. 3684
Steil, B., Brühl, C., Manzini, E., Crutzen, P. J., Lelieveld, J., Rasch, P. J., Roeckner, E., and Krüger, K.: A new interactive chemistry climate model. 1: Present day climatology and interannual variability of the middle atmosphere using the model and 9 years of HALOE/UARS data, J. Geophys. Res., 108, No. D9, 4290, doi:10.1029/2002JD002971, 2003. 3683
WMO (World Meteorological Organisation): Scientific assessment of ozone depletion: 2002, WMO Global Ozone Research and Monitoring, in press, 2003. 3682
Zdundowski, W. G., Welch, R. M., and Korb, G.: An investigation of the structure of typical two-stream methods for calculation of solar fluxes and heating rates in clouds, Beitr. Phys. Atmosph., 53, 147–166, 1980. 3685

Table 1. The coefficients b_i of Eq. (7) for the different species (channels), grouped by wavelength region most important for photolysis.

b_i	species	region
1	$O_3(\rightarrow O(^3P))$, NO_2, NO_3	UV-A or visible
1.3	$ClONO_2$, Cl_2O_2	UV-A
1.4	HOCl	near UV-B
1.5	CH_2O(M), N_2O_5, HNO_4, CH_3O_2H	UV-B
2	CH_2O(R), H_2O_2	UV-B
3	$O_3(\rightarrow O(^1D))$	far UV-B
4	HNO_3	far UV-B
5	O_2, CFC-11, CFC-12, CCl_4, CH_3Cl, CH_3CCl_3, HCl, H_2O, CO_2, N_2O, NO	UV-C

ACPD
3, 3681–3711, 2003

Table 2. Mixing ratios of greenhouse gases, inorganic chlorine, and NO_x emissions of different natural and anthropogenic sources for the "1990" simulations (i.e., the SZA87.5 and the SZA93 run, respectively).

CO_2 (ppmv)	353
CH_4 (ppmv)	1.69
N_2O (ppbv)	310
Cl_y (ppbv)	3.4
NO_x lightning (Tg(N)/year)	5.3
NO_x air traffic (Tg(N)/year)	0.6
NO_x surface (total) (Tg(N)/year)	33.1
NO_x surface (industry, traffic)	22.6
NO_x surface (soils)	5.5
NO_x surface (biomass burning)	5.0

ACPD
3, 3681–3711, 2003

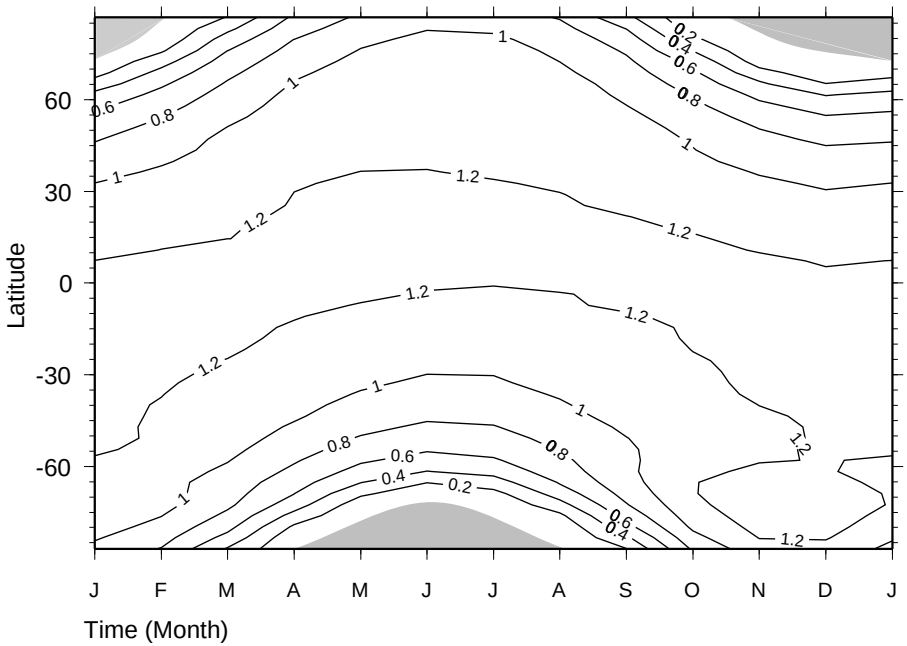

Fig. 1. Photolysis frequencies of Cl_2O_2 [10^{-3} s^{-1}] at 50 hPa in SZA93. Shaded areas indicate polar night. Letters at the *x*-axis denote the beginning months.

ACPD
3, 3681–3711, 2003

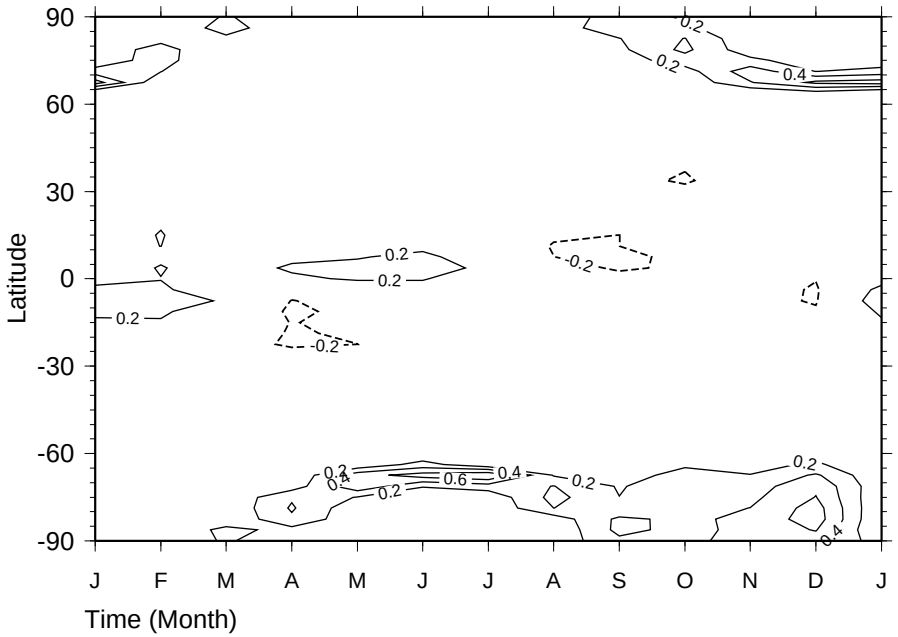

Fig. 2. Differences in photolysis frequencies of Cl_2O_2 [10^{-4} s^{-1}] at 50 hPa between SZA93 and SZA87.5. Positive differences indicate higher photolysis frequencies in SZA93.

ACPD
3, 3681–3711, 2003

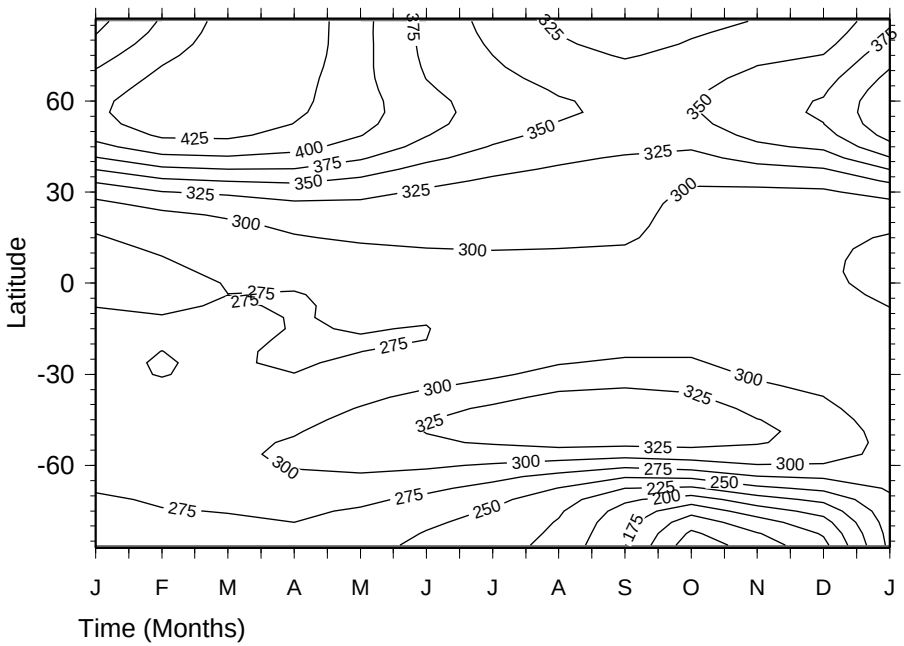

Fig. 3. Modelled climatological zonal mean total ozone (in Dobson Units, DU) taking in account SZAs up to 93° (SZA93). The model results are averaged over 20 simulated years.

ACPD

3, 3681–3711, 2003

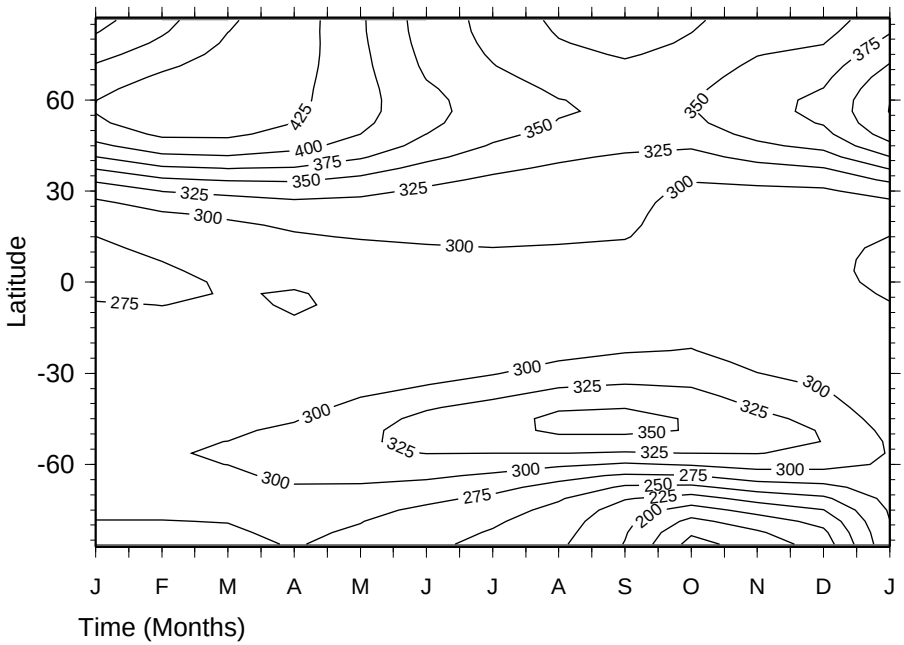

Fig. 4. Same as in Fig. 5, but considering SZAs up to 87.5° only (SZA87.5).

ACPD
3, 3681–3711, 2003

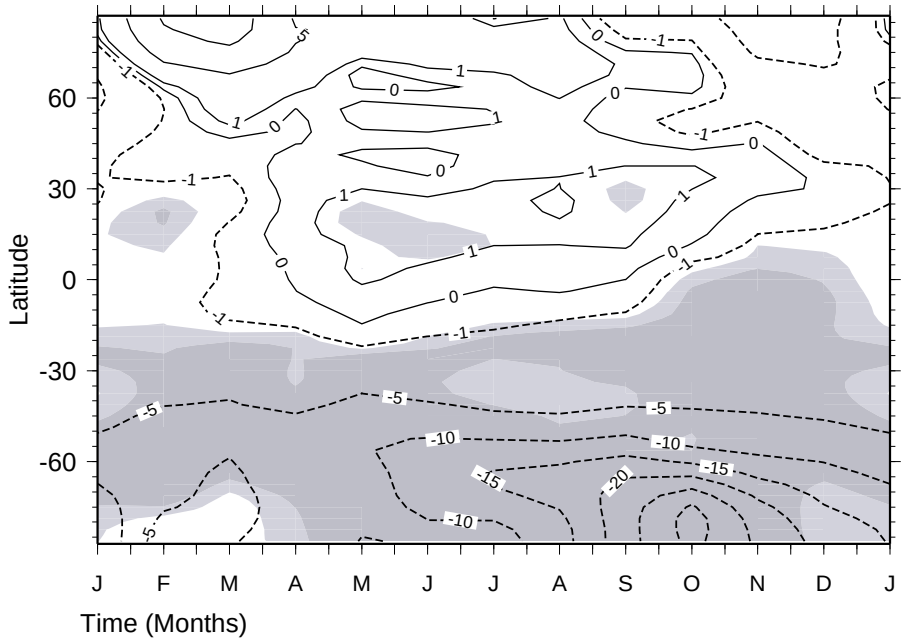

Fig. 5. Changes of total ozone (in DU) between SZA93 and SZA87.5. Negative (positive) values indicate lower (higher) values in SZA93. Dark (light) shaded areas indicate the 99% (95%) significance level (t-test).

ACPD
3, 3681–3711, 2003

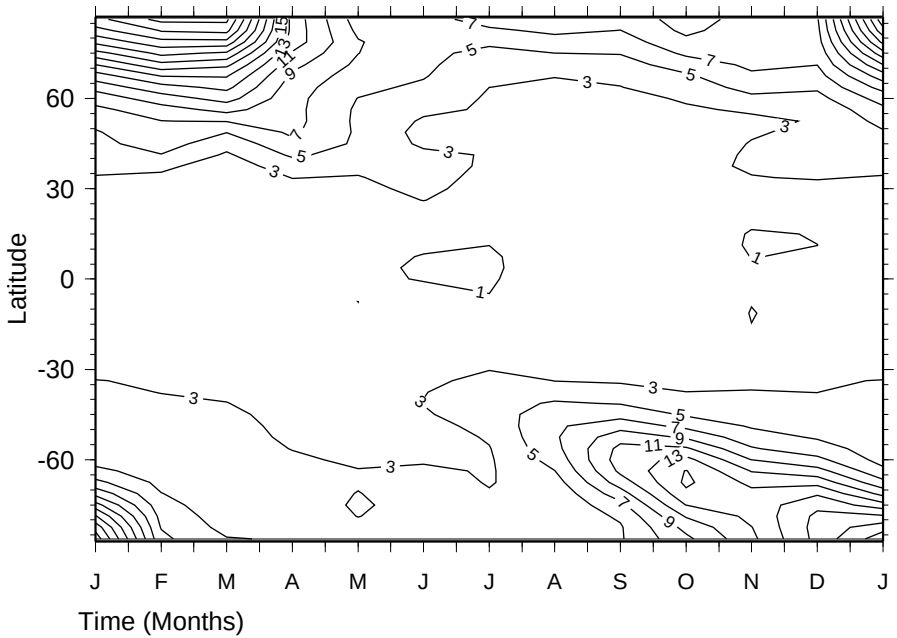

Fig. 6. 1-sigma standard deviation of total ozone (in DU), which is equal in both simulations.

ACPD
3, 3681–3711, 2003

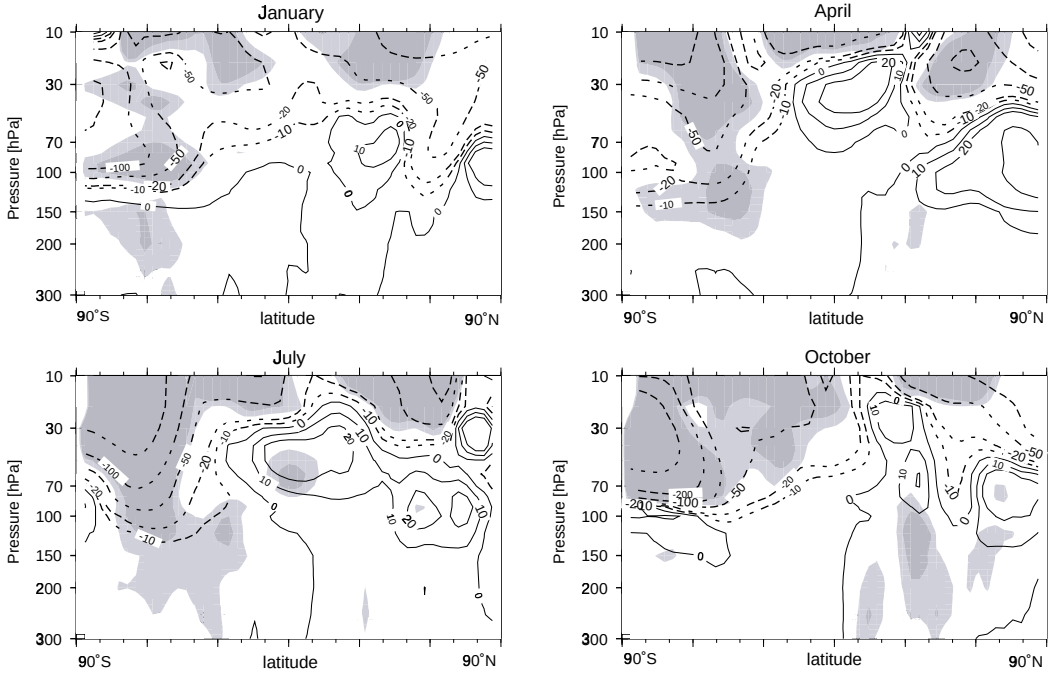

Fig. 7. Changes of climatological zonal mean ozone mixing ratios (ppbv) depending on altitude and latitude for January, April, July, and October. Negative (positive) values indicate lower (higher) values in SZA93. Heavy (light) shaded areas indicate the 99% (95%) significance level (t-test). Isolines are plotted on a logarithmic scale: −500, −200, −100, −50, −20, −10, 0, 10, 20, 50, 100.

ACPD
3, 3681–3711, 2003

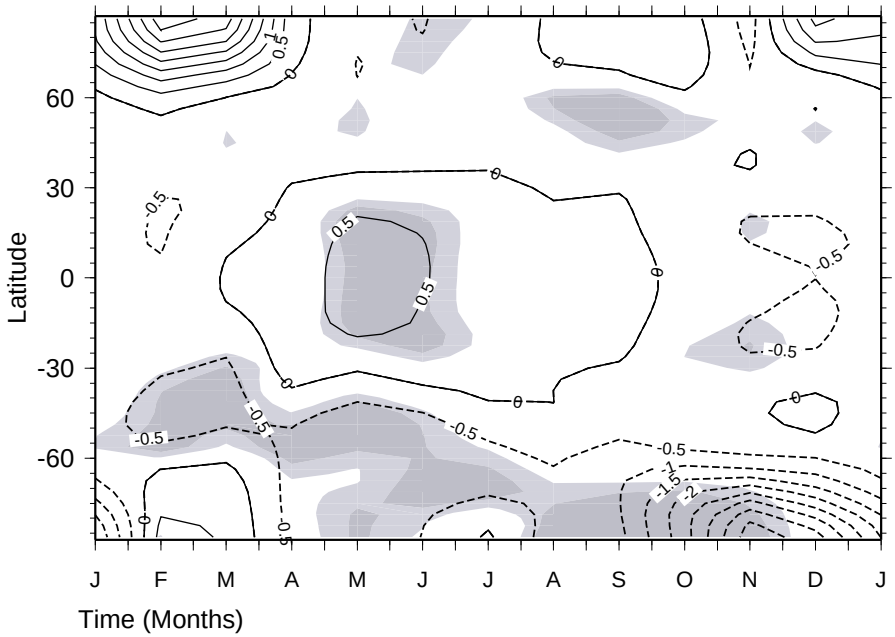

Fig. 8. Changes of climatological mean temperatures (K) at 50 hPa between SZA93 and SZA87.5. Negative (positive) values indicate lower (higher) values in SZA93. Heavy (light) shaded areas indicate the 99% (95%) significance level (t-test).

ACPD
3, 3681–3711, 2003

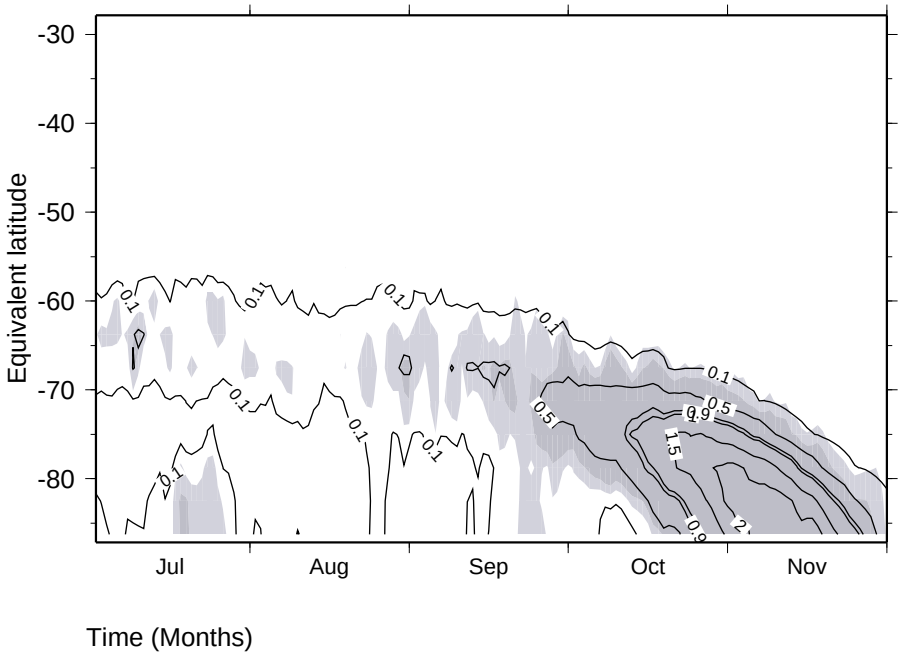

Fig. 9. Changes of the climatological zonal mean PSC I-NAT (ppbv) at 50 hPa in the Southern Hemisphere between SZA93 and SZA87.5. Model data are transformed to the PV-coordinate system. Positive (negative) values indicate higher (lower) values in the SZA93 simulation. Heavy (light) shaded areas indicate the 99% (95%) significance level (t-test).

ACPD
3, 3681–3711, 2003

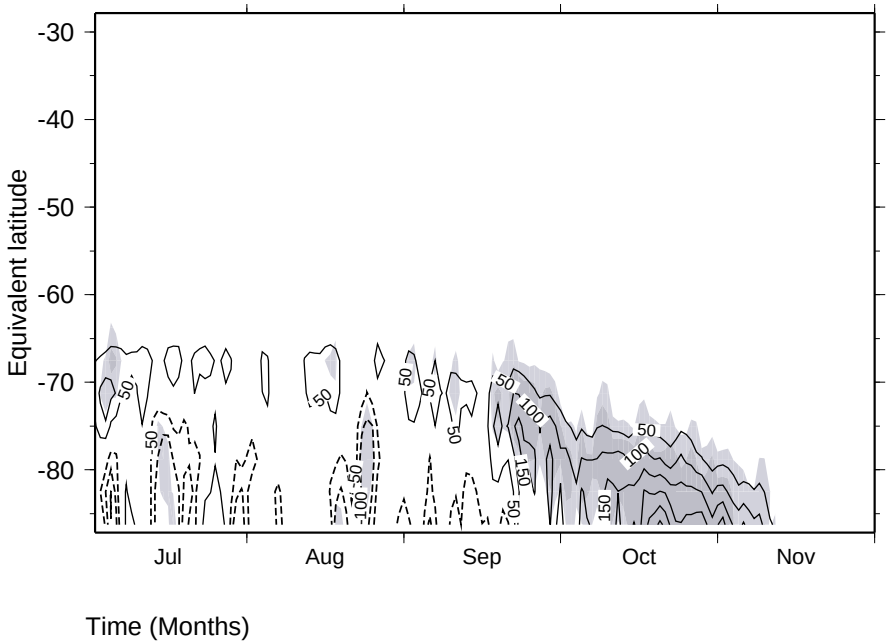

Fig. 10. As Fig. 9, but for PSC II-ICE (pptv).

ACPD
3, 3681–3711, 2003

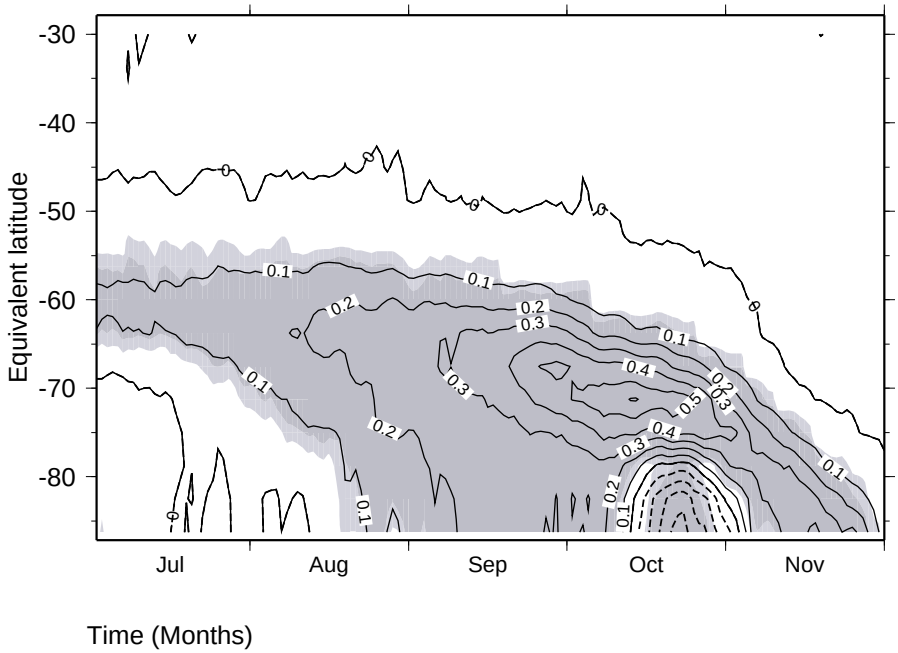

Fig. 11. As Fig. 9, but for ClO_x(ppbv).

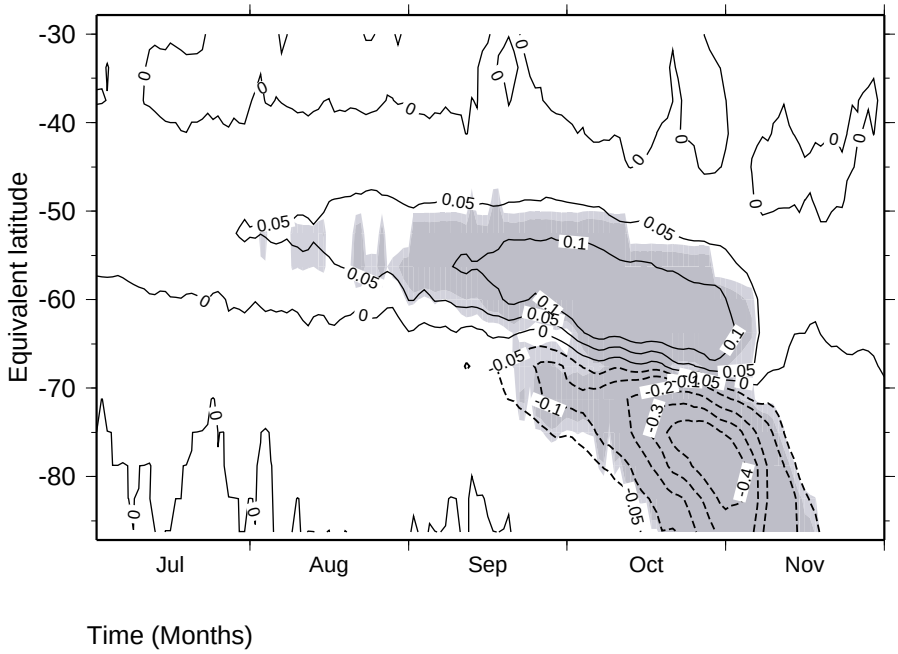

Fig. 12. As Fig. 9, but for $ClONO_2$ (ppbv).

ACPD
3, 3681–3711, 2003

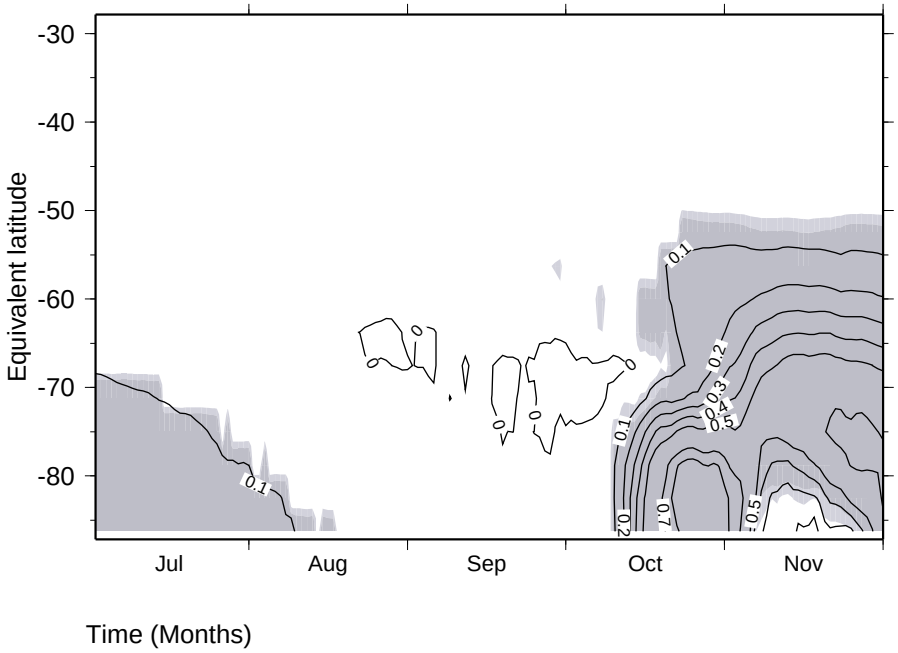

Fig. 13. As Fig. 9, but for HCl (ppbv).

ACPD
3, 3681–3711, 2003